Modal Analysis of a Tensegrity Structure – an experimental study

F. Bossens[*]   R.A de Callafon[†]   R.E. Skelton

Mechanical and Aerospace Engineering
Dynamic Systems and Control Group
University of California, San Diego
9500 Gilman Drive
La Jolla, CA 92093-0411, U.S.A.

Abstract

Tensegrity structures are a special class of lightweight truss structures, where all truss elements are axially loaded and tensile truss elements are made of strings. This paper presents the dynamic analysis of a tensegrity structure by comparing a finite element model with an identified model obtained from experimental data. Experimental data is obtained by placing a three stage tensegrity structure on a shaker table and measuring frequency responses between the moving support and multiple accelerometers placed on the structure. An identified Single-Input-Multiple-Output (SIMO) linear model is found by a SIMO curve fitting of the measured frequency responses. To complete the dynamic analysis, the estimated model along with the identified resonance modes and damping coefficients are used to compare and fine tune a fine element based model.

Keywords: tensegrity structure, dynamic analysis, frequency domain identification, finite element models

1   Introduction

Truss structures, where all truss members are axially loaded and separated in tensile and compressive load carrying members, form a basis for the design of tensegrity structures. As such, tensegrity structures differ from regular trusses by purposefully designing all tensile elements to be strings. The result is a lightweight structure with comparable stiffness properties to regular truss structures. Tensegrity structures were first introduced as an art form in 1948 by Snelson (1965). The work by Fuller (1962) recognized their engineering values.

Tensegrity structures can be designed such that no compressive elements are in direct contact (class 1 tensegrity). Connections between compressive elements are achieved by flexible tensile string elements. For the design of these flexible tensegrity structures much attention has been paid to the static construction and mechanical stability of the structure (Pellegrino and Calladine 1985), (Pellegrino 1989) and (Motro 1992). For a comprehensive static analysis of tensegrity structures one is also referred to Sultan (1999) or Sultan *et al.* (2003). Due to the inherent tunable

---

flexibility of the structure, an important application area of tensegrity structures is vibration isolation, where dynamic analysis of the structure is imperative. Vibration control has already been successfully applied to various cable-structures (Bossens and Preumont 2001, Preumont and Bossens 2000) and can be extended to tensegrity structures.

The work of Furuya (1992) analyzed the vibrational characteristics of some tensegrity structures using finite element programs to investigate the influence of pretension on modal frequencies, concluding that they increase as pretension increases. Skelton and coworkers have proposed analytical formulations for the linear dynamics (Sultan *et al.* 2002) and the nonlinear dynamics (Skelton *et al.* 2001) of certain classes of tensegrity structures.

Experimental studies that complement the development of dynamical models of tensegrity structures for vibration isolation are more scarce in the literature. The work of Motro *et al.* (1986) presents experimental results for the linear dynamical analysis of a 3-bar-9-string tensegrity structure. In this work, harmonic excitation acting on one node is used to measured the dynamic response at the other nodes of the tensegrity structure. However, the results are not used to formulate a dynamic model that can be compared with a finite element analysis.

This paper presents the dynamic analysis of a tensegrity structure using identified models based on experimental data and a finite element model. Experimental data is obtained by placing a three stage tensegrity structure on a shaker table and measuring frequency responses between the moving support and multiple accelerometers placed on the structure. An identified Single-Input-Multiple-Output (SIMO) linear model is found by a weighted SIMO curve fitting of the measured frequency responses. The weighting used in the curve fitting process is chosen such that the dominant resonance modes of the structure are identified. This yields detailed information on the resonance frequency and damping coefficients of each resonance mode that can be verified and fine tuned in a finite element model of the structure presented in this paper.

The outline of the paper is as follows. Section 2 describes the construction of the tensegrity structure, pointing out some critical issues from an engineering point of view. Section 3 summarizes the experimental results, where frequency response measurements are obtained by spectral analysis. In Section 4, a multi-variable curve-fitting technique is applied to the measured frequency reponse data to obtain a multivariable linear model of the structure. The results are combined with a finite element analysis and discussed in Section 5. Finally, Section 6 gives some concluding remarks.

2 Experimental setup

2.1 Tensegrity structure

A three stage tensegrity structure is used as a case study for the analysis presented in this paper. The tensegrity structure is composed of nine compressive members, that appear in pairs of three to form a single stage in the structure. To complete the tensegrity structure, the nine compressive members are connected by a total of 39 tensile members that consist of that Saddle, Vertical and Diagonal (SVD) strings (Masic *et al.* 2002).

For the dynamic analysis, the structure is placed on a shaker table and equipped with accelerometers at the bottom and top of the structure. The tensegrity structure depicted in Figure 1 is said to be of class 1, since each node is connected to 1 compressive member only. The only exception form the top and bottom nodes, where compressive members are connected to rigid supports.

For the design and static analysis of the three stage tensegrity structure in Figure 1, a dedicated constrained optimization is used (Masic *et al.* 2002). Subjected to design considerations, the optimization determines the structural geometry and the corresponding pretension force for each element in the structure. Design considerations may include length of the compressive members and total height of the structure. Details on the constrained optimization technique can be found in Masic *et al.* (2002). For the design of the structure for the experimental set-up discussed in this paper, the following design considerations were taken into account:

- the nodes have to lie on a vertical cylinder with a 0.6 feet diameter

- the bars have a length of 1.5 feet

- the structure must have a total height of 3 feet.

Following the design considerations, the tensegrity structure is composed of nine stainless steel tubes with a length of 1.5 feet, a diameter of 5/16 inch and a 0.030 inch wall thickness. The compressive members are connected by 39 synthetic strings made out of Spectra fiber. A 0.5-inch-thick Plexiglas plate was installed on top of the structure, to place the accelerometers. More details on the construction of the tensegrity structure is outlined in the following sections.

2.2   Adjustable joint

Each node in the tensegrity structure is a joint of a single compressive member and several strings. The design of the string-bar interface represents one of the most critical issues in the construction of a tensegrity structure. To address construction and robustness issues in the design of the structure, the string-bar interface should satisfy the following two requirements:

- String-bar interface should be adjustable to vary the length and tension of strings attached to the interface. The adjustability of strings is beneficial for construction purposes, where pretension has to be adjusted to achieve a desired overall stiffness of the structure.

- String-bar interface should allow for an easy replacement of a string. This requirement is beneficial in case tensile members break during dynamic testing or loading of the tensegrity structure.

The above mentioned considerations led to the design of an end cap for each compressive member, along with an adjustable fixture for the tensile members as indicated in Figure 2. The string-bar interface design consists of a Teflon cap, fitted tightly at the extremities of every compressive member. Subsequently, the various strings are fed through holes drilled in the caps, in such a way that their path contains only obtuse angles. Every string is then winded around a separate adjustable screw, allowing for an easy adjustment of length and tension of the string. In the event that a string actually breaks, it can easily be replaced because it is routed externally to the compressive member.

As a final remark, it can be observed from Figure 2 that the adjustable string-bar interface approximates a single point along the axis of the compressive member where all strings are joined together. In this way, the compressive members do not experience a bending moment due to the strings in tension attached to them.

2.3 Bottom and top support connections

The top and bottom stages of the tensegrity structure respectively have to be attached to a top and bottom and support. The ground support is needed to connect the structure to the shaker table, whereas the top support consists of a plate to mimic a gravity load on the structure and function as a placeholder for the accelerometers.

The connection of the compressive members of the structure to the top and bottom support must prevent the members from translating in the horizontal plane. However, the compressive members should be free to rotate to avoid bending moments on the compressive members, posing the requirements of a ball joint connection. Additionally, the connection should be adjustable for manufacturing purposes. The proposed design is illustrated in Figure 3.

The design solution uses guitar-tuning devices to tighten metal strings connected to the compressive members. The thightening of the metal strings fixes the end of the compressive member to an adjustable slider, creating a system that works like a ball joint. Furthermore, the sliders at the base and top plates can move radially outward or inward, allowing to change the ground points positions and thus the overall structure configuration.

3 Experimental data and spectral analysis

For the dynamic analysis of the three stage tensegrity structure, vibration experiments with a shaker table are used. As indicated in Figure 1, the shaker table provides an acceleration excitation at the bottom support of the tensegrity structure, while acceleration at the top support of the structure is measured at three different locations.

The acceleration measurement y_0 at the base plate of the structure is aligned with the movements of the shaker table and indicated by channel #0 in Figure 4. The location and direction of the three acceleration measurements y_1, y_2 and y_3 at the top plate of the structure are also indicated in Figure 4 by respectively channel #1, channel #2 and channel #3.

From Figure 4 it can be observed that the accelerometers #1 and #2 are placed at the geometric center of the plate, respectively parallel and orthogonal to the direction of excitation. They are expected to be mostly sensitive to translation motion. Accelerometer #3 is oriented parallel to the excitation direction, located 3 inch off-centered. This accelerometer will be used to study both the translational and rotational motion of the structure due to the base acceleration excitation.

To study the dynamic behavior of the structure, a bandlimited white noise of 50Hz is used to excite the shaker table. Measurements of the base plate acceleration y_0 and the three top plate accelerations (y_1, y_2 and y_3) are gathered at a sampling frequency of 500Hz. By means of spectral analysis (Priestley 1981, Ljung 1999) a frequency response function (FRF)

$$G_1(\omega_j) = \frac{\Phi_{y_1 y_0}(\omega_j)}{\Phi_{y_0 y_0}(\omega_j)} \tag{1}$$

between two acceleration signals $y_1(t)$ and $y_0(t)$ is estimated over a linearly spaced frequency grid Ω between 0 and 250 Hz. For a measurement of the acceleration signal consisting of $N = n \times k$ points, the cross-spectrum $\Phi_{y_2 y_1}(\omega)$ (or auto spectrum $\Phi_{y_1 y_1}(\omega)$) in (1) is estimated by a Discrete Fourier Transform (DFT) of an estimated and averaged correlation $\hat{R}_{y_2 y_1}(\tau)$:

$$\Phi_{y_2 y_1}(\omega) = \text{DFT}\{\hat{R}_{y_2 y_1}(\tau)\}, \ \hat{R}_{y_2 y_1}(\tau) := \frac{1}{k} \sum_{m=1}^{k} R_{y_2 y_1}^m(\tau)$$

where

$$R_{y_2y_1}^m(\tau) = \frac{1}{n}\sum_{t=1}^{n} y_2(t+(m-1)n)y_1(t+(m-1)n-\tau), \ m=1,2,\ldots k$$

are the estimated (non-overlapping) correlation functions. For analyzing the bending and torsional modes of the tensegrity structure, the FRF's $G_1(\omega_j)$, $G_2(\omega_j)$ and $G_3(\omega_j)$ between base plate acceleration y_0 and the three top acceleration signals y_1, y_2 and y_3 are estimated using spectral analysis. The amplitude Bode plot of the estimated FRF's between base and top acceleration signals are depicted in Figure 5.

From the estimated FRF's in Figure 5 a few conclusions can be drawn that play a role in the modeling of the structure. Firstly, it should be mentioned that the estimated FRF's are not accurate and reliable for frequencies above 50Hz. This is due to the lack of excitation of the structure above 50Hz with the bandlimited white noise applied to the shaker. Secondly, it can be observed that the structure exhibits multiple bending modes that can be observed in the estimated FRF $G_1(\omega_j)$. The estimated FRF $G_1(\omega_j)$ and $G_3(\omega_j)$ are very similar, as both accelerometers are oriented in the same direction on the top plate. Any differences are due to torsional modes of the structure, that can also be observed in the estimated FRF $G_2(\omega_j)$. Thirdly, it can be seen in the estimated FRF $G_2(\omega_j)$ that the same bending modes also occur in the orthogonal direction of the excitation.

4 Model estimation

4.1 Model parametrization

The FRF's obtained from spectral analysis in Figure 5 will be used to estimate a dynamical model $P(\theta)$. The parametrization of the model $P(\theta)$ and the value of the multi-dimensional real-valued parameter θ will be used to capture the various bending and torsional modes of the structure. The estimation of the parameter θ is done by means of a multivaribale FRF curve fitting (de Callafon *et al.* 1996).

The estimated FRF's in Figure 5 indicate that the bending does not occur solely in the direction of excitation but has both a parallel and a perpendicular component with respect to the direction of excitation. The coupling and direction of the various resonance modes along with their specific damping characteristics should be taken into account in the model $P(\theta)$ of the structure. This can be done formulating a Single-Input-Multi-Output (SIMO) transfer function model

$$\begin{bmatrix} y_1 \\ y_2 \\ y_3 \end{bmatrix} = P(\theta)y_0, \quad P(\theta) := \begin{bmatrix} B_1(\theta) \\ B_2(\theta) \\ B_3(\theta) \end{bmatrix} \cdot \frac{1}{A(\theta)} \tag{2}$$

that is able to capture the coupled vibrational characteristics of the structure from the bottom plate acceleration signal y_0 to the three top plate acceleration signals y_1, y_2 and y_3.

The parametrization of the model $P(\theta)$ in (2) is a special case of a Matrix Fraction Description (de Callafon *et al.* 1996), where $A(\theta)$ denotes the common denominator polynomial of the transfer function model $P(\theta)$ and $B_n(\omega_j)$, $n = 1,\ldots,3$ denotes the numerator polynomial for each output signal. The parametrization can be extended to include multiple input acceleration signals (de Callafon *et al.* 1996) but for the purpose of the experiments discussed in this paper, only one input acceleration signal is considered. The resulting common denominator allows the

coupled modeling of resonance modes observed in the three measured output signals y_1, y_2 and y_3.

4.2 Curve fitting

The parameter θ in the linear dynamical model $P(\theta)$ of (2) is found by curve fitting the estimated FRF (de Callafon *et al.* 1996). The curve fitting of the estimated FRF is addressed by evaluating the frequency response of the model $P(\theta, \omega_j)$ over the same frequency grid Ω and defining an additive curve fit error

$$E_a(\omega_j, \theta) := \left[\begin{bmatrix} G_1(\omega_j) \\ G_2(\omega_j) \\ G_3(\omega_j) \end{bmatrix} - \begin{bmatrix} B_1(\theta, \omega_j) \\ B_2(\theta, \omega_j) \\ B_3(\theta, \omega_j) \end{bmatrix} \cdot \frac{1}{A(\theta, \omega_j)} \right]$$

To tune the additive curve fit error $E_a(\omega)$, an additional frequency dependent weighting $W_n(\omega_j)$, $n = 1, \ldots, 3$ can be used to define the (weighted) curve fit error

$$E(\omega_j, \theta) := \left(\begin{bmatrix} W_1(\omega_j) \\ W_2(\omega_j) \\ W_3(\omega_j) \end{bmatrix} .* \left[\begin{bmatrix} G_1(\omega_j) \\ G_2(\omega_j) \\ G_3(\omega_j) \end{bmatrix} - \begin{bmatrix} B_1(\theta, \omega_j) \\ B_2(\theta, \omega_j) \\ B_3(\theta, \omega_j) \end{bmatrix} \cdot \frac{1}{A(\theta, \omega_j)} \right] \right) \tag{3}$$

where $.*$ denotes the Schur product: an element by element multiplication. Estimation of a parameter $\hat{\theta}$ in the model $P(\theta)$ of (2) is done by a least squares minimization

$$\hat{\theta} := \arg \min_\theta \sum_{j=1}^{n} \text{tr}\{E(\omega_j, \theta) E^*(\omega_j, \theta)\} \tag{4}$$

of the weighted curve fit error over the frequency grid Ω. In de Callafon *et al.* (1996) a recursive linear method is proposed to approximate the non-linear least squares optimization of (4). The results of the curve fitting procedure are depicted in the following section.

4.3 Model estimation results

The results of the SIMO model estimation using the multivariable curve fitting has been depicted in the Bode plot of Figure 6. The frequency dependent weighting $W_n(\omega_j)$, $n = 1, \ldots, 3$ in (3) was chosen as the inverse of the FRF data $G_n(\omega_j)$, $n = 1, \ldots, 3$ to minimize a relative curve fit error. Additionally, the frequency dependent weighting was chosen small beyond 40Hz to concentrate the modeling on the low frequency resonance modes of the structure.

The estimated model $P(\hat{\theta})$ is a SIMO 14th order model that captures the first 7 dominant resonance modes of the tensegrity structure. A good fit of the estimated FRF is obtained and the 7 resonance modes capture the coupling of the vibration modes of the structure in all 3 top acceleration signals. The phase Bode plot in Figure 6 shows that the phase of $P(\hat{\theta}, \omega_j)$ is slightly higher than the phase obtained from spectral analysis of the experimental data, and this trend increases with the frequency. This phase difference is due to a constant delay introduced in the experimental data by the AD converter at each time step. At frequency f, a delay of ΔT in the AD converter will introduce a phase lag of $360 f \Delta T$ in the phase Bode plot.

Next to the accurate estimation of the first 7 resonance modes of the tensegrity structure, the model $P(\hat{\theta})$ also gives insight in the undamped resonance frequency ω and damping ratio β for

each resonance mode. This is done by examining the location of the (complex conjugate) zeros s_n, $\bar{s}_n$

$$A(\hat{\theta}, s_n) = 0, \ s_n = \bar{s}_n, \ n = 1, \ldots, 7$$

of the 14th order denominator polynomial. For each complex conjugate pole pair s_n, $\bar{s}_n$ we have

$$\omega_n = \frac{|s_n|}{2\pi} \ \text{Hz}, \ \beta_n = -\frac{\text{Re}\{s_n\}}{|s_n|}$$

The results are summarized in Table 1. It can be observed that all resonance modes exhibit a fairly low damping. Moreover, the structure exhibits two low frequency bending modes that are close together. Development of the finite element model gives more insight in the shape of the resonance modes of this tensegrity structure.

5   Finite element analysis

5.1   Mass and stiffness matrix formulation

Since all members of the tensegrity structure experience only axial loads, the formulation of a dynamical model is less complicated than for truss structures with members exhibited to bending and torsional loads. This unidirectional loading of members is a distinct advantage for modeling purposes since it eliminates many nonlinearities that influence the analysis of other structural truss structures.

For the development of a finite-element model (FEM) of the three stage structure each element in the structure is characterized by the following local mass and stiffness matrices (Cook *et al.* 2002):

$$M_{loc} = \frac{m}{6} \begin{bmatrix} 2 & 0 & 0 & 1 & 0 & 0 \\ 0 & 2 & 0 & 0 & 1 & 0 \\ 0 & 0 & 2 & 0 & 0 & 1 \\ 1 & 0 & 0 & 2 & 0 & 0 \\ 0 & 1 & 0 & 0 & 2 & 0 \\ 0 & 0 & 1 & 0 & 0 & 2 \end{bmatrix} \quad K_{loc} = \begin{bmatrix} k & 0 & 0 & -k & 0 & 0 \\ 0 & T/L & 0 & 0 & -T/L & 0 \\ 0 & 0 & T/L & 0 & 0 & -T/L \\ -k & 0 & 0 & k & 0 & 0 \\ 0 & -T/L & 0 & 0 & T/L & 0 \\ 0 & 0 & -T/L & 0 & 0 & T/L \end{bmatrix} \quad (5)$$

where each element in the structure is characterized by a mass m, a length L, a linear longitudinal stiffness k and a pretension force T. The pretension force T for each element is found by a standard static equilibrium analysis of the structure. The mass and stiffness matrix in (5) are formulated in a cartesian coordinate system $\{xyz\}$ where x is aligned with the longitudinal direction of the specific compressive or tensile member in the tensegrity structure.

As for any pretensioned structure, the stiffness matrix contains both a structural stiffness k and a pretension T/L contribution. The global mass and stiffness matrices M and K are obtained by adding up the contributions from individual elements, expressed in the entire set of degrees-of-freedom, in a common cartesian system of coordinates. The spectral decomposition of matrix $M^{-1}K$ then yields the natural frequencies $\bar{\omega}_n$ and corresponding mode shapes ϕ_n of the FEM for each of the resonance modes of the structure.

5.2 Fine tuning of finite element model

Some parameters in the FEM of the tensegrity structure are not known accurately beforehand. Examples of unknown parameters are the tensile member (string) cross-section area and elasticity modulus, the exact level of pretension in the structure and the mass repartition of the top plate attached to the structure.

With the experimental data and the estimated model $P(\hat{\theta})$, unknown parameters α of the FEM can be fine tuned to match the observed resonance frequencies ω_n listed in Table 1. This is done by formulating a minimization in which the parameter α is used to minimize the difference between the undamped natural frequencies $\bar{\omega}_n$ of the FEM and ω_n of $P(\hat{\theta})$:

$$\hat{\alpha} = \arg \min_{\alpha} \Delta_{\omega}^{T}(\alpha)\Delta_{\omega}(\alpha), \ \Delta_{\omega}(\alpha) := \begin{bmatrix} \bar{\omega}_1(\alpha) - \omega_1 \\ \bar{\omega}_2(\alpha) - \omega_2 \\ \vdots \\ \bar{\omega}_n(\alpha) - \omega_n \end{bmatrix} \tag{6}$$

In general, the dependency of the resonance frequencies $\bar{\omega}(\alpha)$ of the FEM on the unknown parameters α is non-linear. However, the function $\bar{\omega}(\alpha)$ is differentiable in α, as small perturbations of the unknown parameter α will lead to bounded perturbations of the resonance frequencies $\bar{\omega}_n$ in the FEM.

As a result, the non-linear minimization of (6) can be tackled by a Gauss-Newton iteration to find a local minimum. For a Gauss-Newton optimization, only the gradient of $\Delta_{\omega}(\alpha)$ with respect to α needs to be computed. The gradient can be approximated by numerical implementation using small step changes of the parameter α. The optimization was used to match the first four natural frequencies $\bar{\omega}_n$ of the FEM with undamped natural frequencies ω_n of the identified model $P(\hat{\theta})$ (Table 1). Their corresponding modal shape is represented in Figure 7.

These modal shapes are in agreement with the observations of the identification results presented in Section 4, where the modal shapes (bending or torsion) where estimated from the FRFs of Figure 5. As a final remark it can be noted that the optimization increases in computational complexity in the case the number n of resonance frequencies to be matched in (6) is increased. The possibility to encounter a local minimum during the optimization of (6) increases for large number of resonance frequencies to match. As a result, for higher-order modes, no satisfactory match between the resonance frequencies of the FEM and the model $P(\hat{\theta})$ could be obtained. The discrepancy between the models is also attributed to uncertain properties of the actual structure. The uncertain properties may include:

- The unknown pretension of the tensile members in the tensegrity structure.

- The tightened steel strings used to fix the ground joints induce some local rotational stiffness, not considered in the model.

- Gravity effects induced by the members of the tensegrity structure were neglected in the FEM.

Despite these uncertain properties of the actual structure, a satisfactory match for the first four resonance frequecies is obtained. The resonance frequency of the first two bending and torsion modes obtained by the FEM match the resonance frequencies found experimentally in the identified model $P(\hat{\theta})$.

5.3 Mechanism in tensegrity structure

With the experimentally verified finite element model, the existence of a 'soft mode' in the tensegrity structure (Calladine and Pellegrino 1991) can be illustrated. The presence of a soft mode indicates an infinitesimal mechanism which is not associated to any deformation energy of the tensegrity structure. This means that members of the structure are allowed to move without deformation. Soft modes are also characterized by the existence of a right null-space for the stiffness matrix K, when pretension terms T/L are cancelled (Calladine and Pellegrino 1991).

In order to detect the presence of a soft mode, the resonance frequency of the first four modes of the FEM is computed as a function of the pretension level in the tensegrity structure. Figure 8 shows the change in natural frequency for increasing pretension level. For comparison of the different pretension levels, the pretension shown in Figure 8 is the maximum level of pretension found in (one of) the tensile members of the structure. The pretension in all other members of the structure is related to this maximum level by a constant factor, as the geometry of the structure does not change.

The vertical line in Figure 8 indicates the natural frequencies of the initial FEM that was tuned towards the actual measurements listed in Table 1. As pretension approaches zero, it can be observed that the first natural frequency also approaches zero. In other words, this mode is associated with no deformation energy and can be qualified as the soft mode of the structure. Pretensioning is thus the only way to increase the stiffness of the tensegrity structure when such a soft modes exist. Note that soft modes can be avoided by adding more strings to the tensegrity structure at proper locations.

6   Concluding remarks

This paper presents the dynamic analysis of a three stage tensegrity structure by comparing a finite element model with an identified model obtained from experimental data. The results presented in this paper indicate that a linear model can properly portray the dynamics of a tensegrity structure. Using vibration experiments obtained by base excitation of the structure and measuring multiple accelerometers placed on the structure, a single-input-multiple-output linear model is found by multivariable curve fitting of the measured frequency responses. The identified undamped resonance frequencies of the model are used to fine tune a finite element model of the structure and match the first four modal frequencies of the structure. The predicted modal shapes of the structure were in agreement with the experimental data and the identified model. This study will serve as background for future work concerning the design and implementation of tensegrity structres for vibration isolation.

7   Acknowledgements

References

Bossens, F. and A. Preumont (2001). Active tendon control of cable-stayed bridges: A large scale demonstration. *Journal of Earthquake Engineering and Structural Dynamics.* **30**, 961–979.

Calladine, C.R. and S. Pellegrino (1991). First order infinitesimal mechanisms. *International Journal of Solids and Structures.* **27**, 505–515.

Cook, R.D., D.S. Malkus, M.E. Plesha and R.J. Witt (2002). *Concepts and Applications of Finite Element Analysis.* Wiley & Sons.

de Callafon, R.A., D. Roover and P.M.J. Van den Hof (1996). Multivariable least squares frequency domain identification using polynomial matrix fraction descriptions. In *Proc. 35th IEEE Conference on Decision and Control.* Kobe, Japan. pp. 2030–2035.

Fuller, R. Buckminister (1962). *Tensile–integrity structures.* US Patent. 3,063,521.

Furuya, H. (1992). Concept of deployable tensegrity structures in space applications. *International Journal of Space Structures.* **7**(2), 143–151.

Ljung, L. (1999). *System Identification: Theory for the User (second edition).* Prentice-Hall, Englewood Cliffs, New Jersey, USA.

Masic, M.R., R.E. Skelton and P.E. Gill (2002). Algebraic tensegrity design framework. *Internal Report, UCSD, MAE Department.*

Motro, R. (1992). Tensegrity systems: The state of the art. *International Journal of Space Structures.* **7**(2), 75–83.

Motro, R., S. Najari and P. Jouanna (1986). Static and dynamic analysis of tensegrity systems. In *Proceedings of the ASCE International Symposium.* New-York: Springer-Verlag.

Pellegrino, S. (1989). Analysis of prestressed mechanisms. *International Journal of Solids and Structures.* **26 (12)**, 1329–1350.

Pellegrino, S. and C.R. Calladine (1985). Matrix analysis of statically and kinematically indeterminate frameworks. *International Journal of Solids and Structures.* **22(4)**, 409–428.

Preumont, A. and F. Bossens (2000). Active tendon control of vibration of truss structures: Theory and experiments. *Journal of Intelligent Material Systems and Structures.* **11**(2), 91–99.

Priestley, M.B. (1981). *Spectral Analysis and Time Series.* Academic Press, London, England.

Skelton, R.E., J.P. Pinaud and D.L. Mingori (2001). Dynamics of the shell class of tensegrity structures. *Journal of the Franklin Institute.* **338/2-3**, 255–320.

Snelson, K. (1965). Continuous tension, discontinous compression structures. *U.S. Patent 3,169,611.*

Sultan, C. (1999). *Modeling, design, and control of tensegrity structures with applications.* Ph.D. Dissertation, Purdue University, School of Aeronautics and Astronautics, West Lafayette.

Sultan, C., M. Corless and R.E. Skelton (2002). Linear dynamics of tensegrity structures. *Engineering Structures.* **24**, 671–685.

Sultan, C., M. Corless and R.E. Skelton (2003). The prestressability problem of tensegrity structures. some analytical solutions. *To appear in International Jounal of Solids and Structures.*

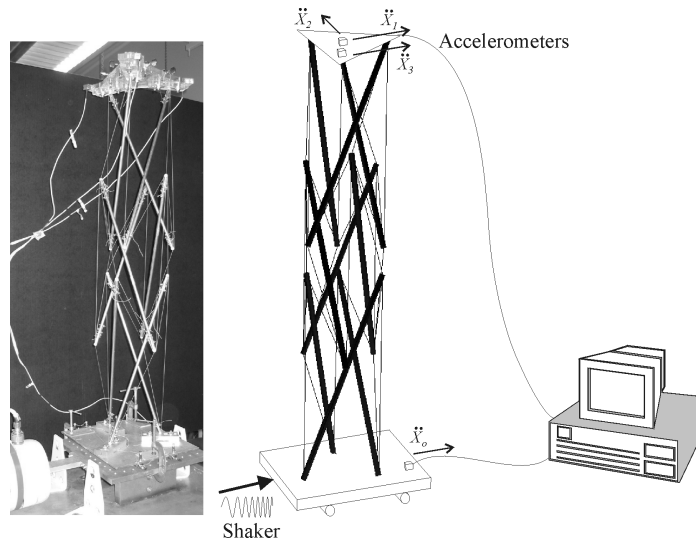Figure 1: Experimental setup of three stage tensegrity structure consisting of nine compressive bars and 39 strings placed on a shaker table
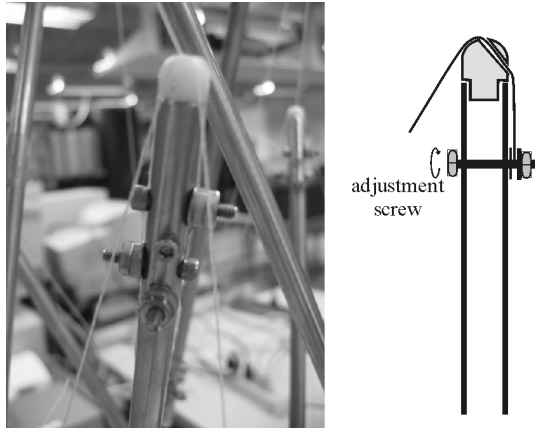
Figure 2: Adjustable string-bar interface design
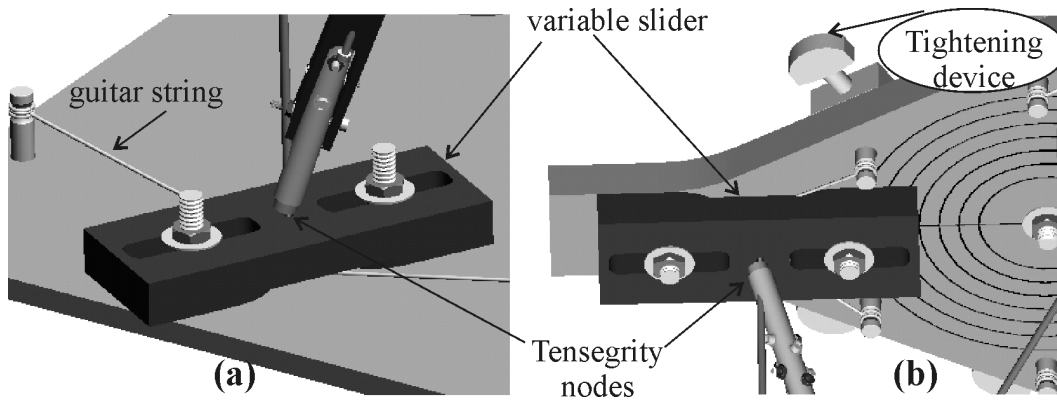
Figure 3: Joint design for bottom support (left) and top support (right).
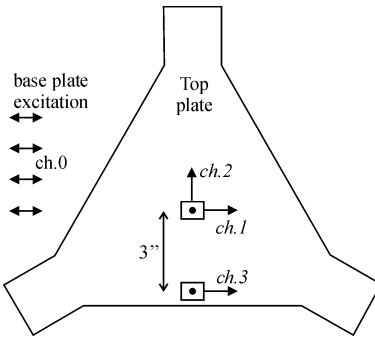
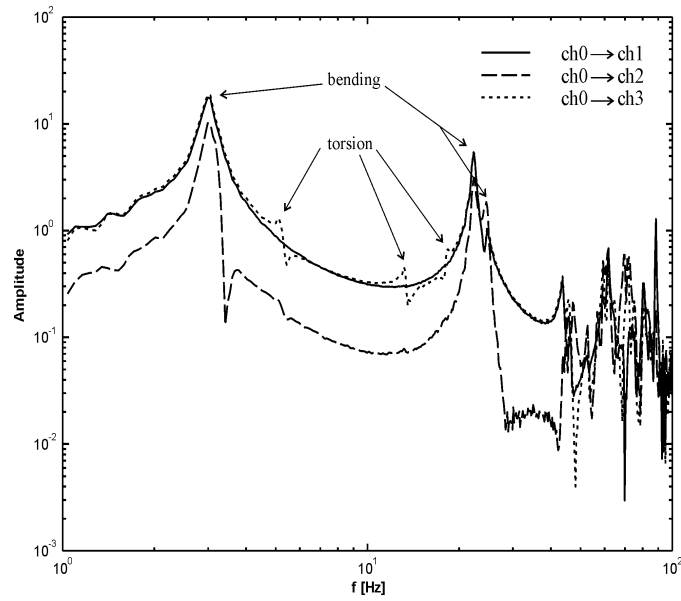Figure 4: Location of accelerometers on top plate of the tensegrity structure

Figure 5: Bode amplitude plot of the estimated frequency response function (FRF) $G_1(\omega_j)$ (solid), $G_2(\omega_j)$ (dashed) and $G_3(\omega_j)$ (dotted) between base and top acceleration signals
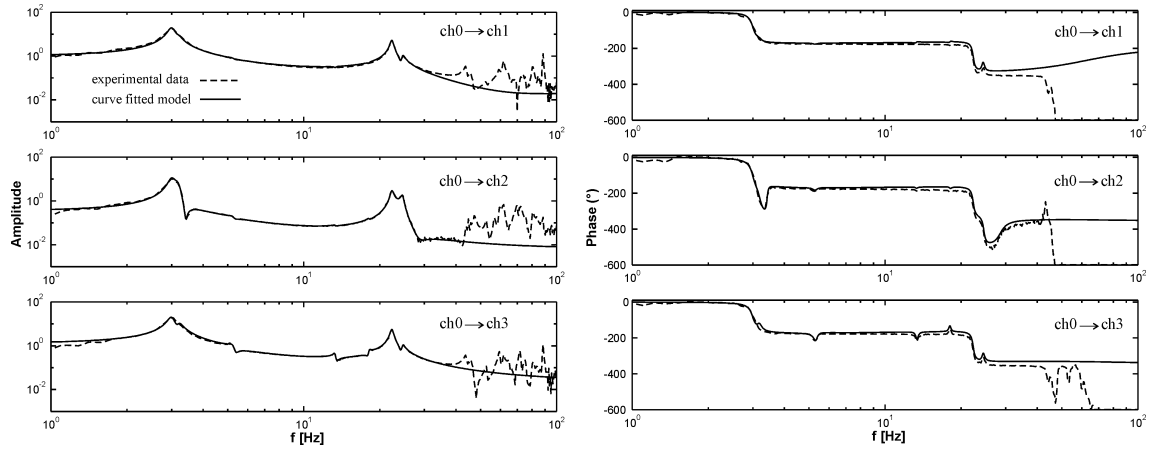
Figure 6: Amplitude Bode plot (left) and phase Bode plot (right) of the estimated FRF $G_1(\omega_j)$, $G_2(\omega_j)$ and $G_3(\omega_j)$ (dashed) and curve fitted 14th order SIMO model $P(\hat{\theta}, \omega_j)$ (solid)

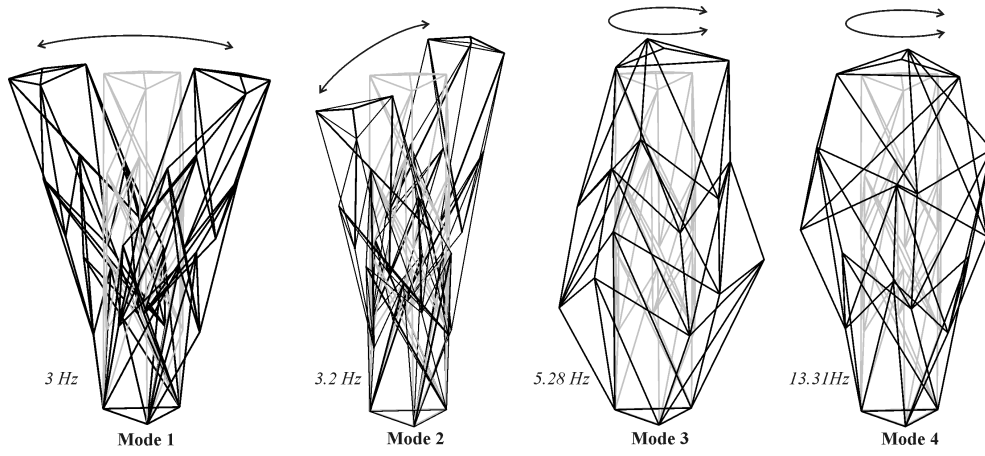3 Hz **Mode 1**   3.2 Hz **Mode 2**   5.28 Hz **Mode 3**   13.31Hz **Mode 4**

Figure 7: Modal shape of the first 4 natural frequencies of the FEM
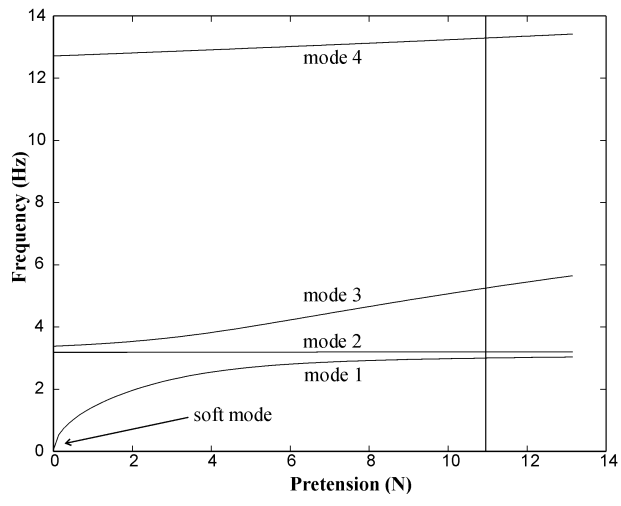
Figure 8: Variation of the first 4 natural frequencies with the level of pretension in the structure

Mode n	ω_n [Hz]	β_n [%]	Description
1	3.00	3.09	bending 1
2	3.20	2.50	bending 2
3	5.28	2.44	torsion 1
4	13.31	1.24	torsion 2
5	18.10	1.14	torsion 3
6	22.31	1.45	bending 3
7	24.56	1.41	bending 4

Table 1: Undamped natural frequency ω_n and associated damping coefficient β_n of the 7 resonance modes modeled in the estimated SIMO model $P(\hat{\theta})$